Contributed Paper

Pedestal Characteristics of H-Mode Plasmas in JT-60U and ASDEX Upgrade

URANO Hajime[i)], KAMADA Yutaka[i)], TAKIZUKA Tomonori[i)], SUTTROP Wolfgang[ii)], HORTON Lorne [ii)], LANG Peter [ii)], KUBO Hirotaka[i)], OYAMA Naoyuki[i)], TAKENAGA Hidenobu[i)] and ASAKURA Nobuyuki[i)]

[i)]*Naka Fusion Research Establishment, Japan Atomic Energy Research Institute, Ibaraki 311-0193, Japan*

[ii)]*Max-Planck-Institut für Plasmaphysik, Garching 85748, Germany*

(Received 23 November 2004 / Accepted 8 February 2005)

The role of the pedestal structure in ELMy H-mode plasmas for the core energy confinement and for the ELM energy losses were investigated in two tokamak-type devices, JT-60U and ASDEX Upgrade. The confinement degradation seen at higher densities is attributed to the reduction of the pedestal temperature limited by the ELM activities and the stiffness of the temperature profiles. In high triangularity or impurity seeded H-modes, in which higher energy confinement is generally achieved, a higher pedestal temperature is obtained by improving the edge MHD stability or the density profile peaking, respectively. The upper bound of the ELM energy loss is characterized by the pedestal energy. The ELM energy loss can become smaller at fixed pedestal energy when the pedestal collisionality is raised. Raising the pedestal collisionality also enhances the inter-ELM perpendicular transport loss and reduces the ELM loss power fraction. In ASDEX Upgrade, the continuous pellet injection is shown to effectively mitigate ELM losses while preserving the core confinement quality. In JT-60U, the operation regime of grassy ELM is investigated and shown to achieve highly integrated performance of high energy confinement with small ELMs in the low collisionality regime.

Keywords:

Pedestal, H-mode, ELM, profile stiffness, energy confinement, JT-60U, ASDEX Upgrade

1. Introduction

Sufficiently heated H-mode plasmas, which are characterized by the formation of an edge transport barrier, are generally accompanied by the appearance of edge-localized mode (ELM) instabilities driven by a large edge pressure gradient that causes periodic expulsion of plasma energy and particles [1-4]. ELMs allow sustainment of steady-state phases with exhaust of impurities such as helium ash [5-8]. ELMy H-mode experiments performed in many divertor tokamaks have also demonstrated favorable energy confinement. ELMy H-mode has therefore been adopted as the reference regime for inductive operation of the International Thermonuclear Experimental Reactor (ITER) [9]. Significant progress has been made on the experimental research on ELMy H-modes, and several indispensable restrictions in a reactor relevant regime have been revealed. There are two main constraints strongly related to the H-mode pedestal properties for the design of a fusion reactor. (i) One is the crucial energy confinement degradation that is generally seen as the density is raised. High density operation with improved energy confinement is essential in order for a tokamak reactor to produce sufficiently high fusion power. ITER is also envisaged to operate at a high density close to the Greenwald density. It is therefore imperative that we clarify the dominant causes of this degradation and extend the H-mode operation regime towards the improved energy confinement and higher fusion power gain. (ii) The other constraint is a potentially excessive heat load generated by ELM bursts. The periodic relaxation of the edge pressure gradient in ELMy H-mode results in a pulse of energy and particles transported across the separatrix to the scrape-off layer (SOL) and eventually into the divertor. The energy loss produced by ELM bursts can raise the surface temperature above the ablation threshold and increase erosion of the divertor targets to the point where the lifetime of the component becomes unacceptably short [10-13]. Therefore, it is also crucial that we characterize the ELM losses from the viewpoint of the pedestal parameters.

In this article, we examine the role of the pedestal properties in H-mode plasmas on the core energy confinement and on the ELM energy losses using two tokamak devices, JT-60U and ASDEX Upgrade. This paper is organized as follows. First, the effects of the H-mode pedestal on the core energy confinement are described in Sec. **2**. By dividing the

author's e-mail: urano@naka.jaeri.go.jp

This article is based on the invited talk at the 21th JSPF Annual Meeting (2004, Shizuoka).

thermal plasma energy into core and pedestal components, the main cause of the confinement degradation at high densities is identified. The characteristics of both the core and pedestal profiles observed in these two devices indicate several possible operating methods, such as high triangularity configuration or impurity seeding, that would greatly improve the energy confinement properties. It is quantitatively shown that the observed high core confinement in high triangularity or impurity seeded H-mode is achieved through the same mechanism as described above for the standard H-mode with high energy confinement. In Sec. **3**, the characteristics of the ELM energy losses are presented. The dependence of ELM losses on the pedestal parameters is described from the viewpoint of the energy balance. The active ELM control by continuous pellet injection is considered as a desirable technique for highly integrated performance of high energy confinement accompanied by small ELMs. As a means of achieving pedestal conditions identical to those in plasma with gas puff and with pellet injection, the mitigation of ELM loss during the fully pellet-controlled phase is also demonstrated in this Section. Finally, conclusions are given in Sec. **4**.

2. The Role of the Pedestal Structure in Energy Confinement

2.1 The thermal energy confinement in core and pedestal plasmas

While it has generally been seen that high density ELMy H-mode regimes have diminished core plasma confinement quality [14-16], the role of the pedestal structure determined by the ELM activities is considered to be significant for the thermal transport of the plasma core. In this Section, to identify the effect of the pedestal structure on the core energy confinement, we consider the thermal energy separated into core and pedestal components. In an offset non-linear (ONL) scaling for ELMy H-mode confinement [17], the pedestal component determined by the MHD stability of ELMs and the core component governed by the gyro-Bohm-like transport are separated as follows:

$$W_{th}^{ONL} = 0.082\kappa R_p a_p I_p B_t b^{-0.1} + 0.043 R_p^{1.3} a_p I_p^{0.6} n_e^{0.6} b^{-0.15} P_L^{0.6}, \quad (1)$$

with $b \equiv B_t R_p^{1.25}$, where W_{th} denotes the thermal stored energy, κ the plasma elongation, R_p the major radius, a_p the minor radius, I_p the plasma current, B_t the toroidal magnetic field, n_e the line averaged electron density in the unit of 10^{19} m^{-3}, and P_L the loss power given by $P_{abs} - dW/dt$, where P_{abs} is the absorbed power. The first and second term represent the pedestal and core components, respectively (See Fig. 1(a)). Figure 1(b) shows the energy confinement enhancement factor (H_H-factor) evaluated by the ONL scaling as a function of the line averaged electron density normalized to the Greenwald density limit in JT-60U [18]. The operation parameters in these plasmas are I_p = 1.8 MA, B_t = 3.0 T, R_p = 3.25 m, a_p = 0.83 m, $\kappa \sim 1.5$, and $\delta \sim 0.16$, where δ is the plasma triangularity. It is observed that the pedestal H_H-factor remains constant in the range of 0.5–0.7 over the wide density

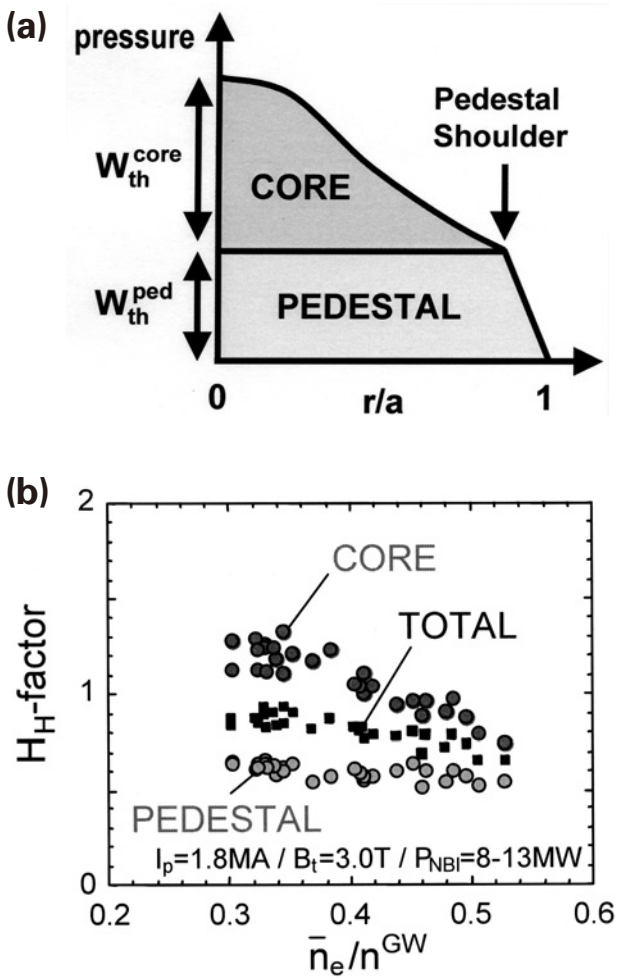

Fig. 1 (a) Schematic representation of the thermal energy stored in the pedestal plasma, W_{th}^{ped}, and in the core plasma, W_{th}^{core}. (b) The enhancement factors for the total, core and pedestal components during the type-I ELMy H-mode based on the offset nonlinear scaling are plotted as a function of the line-averaged electron density normalized to the Greenwald density.

range of n_e/n_{GW} = 30–53%, while the core H_H-factor decreases significantly from 1.3 to 0.8 with increasing density. This result is caused by the saturation of the thermal energy stored in the plasma core W_{th}^{core} for the increase of density, in spite of the results predicted from the scaling ($W_{th}^{core} \propto n_e^{0.6}$) described as Eq. (1). Attention must be drawn to the saturation of W_{th} with density. Based on this finding, it is clear that the confinement degradation seen at high densities is attributed to the deterioration of the core confinement. The answer to the question of why the core H_H-factor decreases with density is given in Sec. **2.3** by analyzing the profiles of density and temperature.

2.2 The operational boundary in the pedestal region in ELMy H-mode plasmas

In this Section, the density dependence of the pedestal structure is discussed. Figure 2(a) shows the classification of ELM behavior in the space of the density and temperature at the pedestal shoulder. The arrow (i) indicates the high density

discharge (n_e = (3.0–3.8)×10^{19} m^{-3}). The electron pedestal pressure p_e^{ped} ($\propto n_e^{ped} T_e^{ped}$) increases throughout the type-III ELM region with additional heating power after the L-H transition, and then the type-I ELMs appear when p_e^{ped} increases further with high power heating. In the type-I ELMy H-mode phase, the increase of n_e^{ped} accompanies the decrease of T_e^{ped} so that the thermal energy stored in the pedestal is kept constant, as seen in Fig. 1(b). The arrow (ii) indicates the low density discharge without the type-III ELMy phase (n_e = (1.5–2.5)×10^{19} m^{-3}). Since the L-H transition occurs at quite a low density, the ELM free phase is sustained and the type-III ELM region is completely avoided. However, the discharges for both the cases (i) and (ii) reach the same boundary of p_e^{ped}, which corresponds to the type-I ELMy H-mode. The features of the edge operation diagram are exactly the same in ASDEX Upgrade [19]. The limit of p_{ped} associated with type-I ELMs generally corresponds to a hyperbolic curve in n-T space at the pedestal shoulder. In other words, p_{ped} stays roughly constant ($n_{ped} T_{ped}$ ~ const.) for fixed I_p, B_t and plasma configuration.

Therefore, as the density is raised, the saturation of p_{ped} imposed by the destabilization of type-I ELMs forces a crucial reduction in the pedestal temperature. The reduced pedestal temperature is a key parameter for the degradation of the core energy confinement in the high density regime. Figure 2(b) plots the H_H-factors based on the ONL scaling as a function of the ion pedestal temperature [18]. With increasing (or decreasing) pedestal temperature, the core H_H-factor increases (or decreases). This result implies that the core temperature profile is strongly affected by the pedestal temperature, suggesting that there exists a large transport structure under which the core temperature is strongly influenced by a boundary value.

2.3 Stiffness of the temperature profile

In this Section, for the purpose of evaluating the edge-core relationship in ELMy H-mode plasmas, we analyze the density dependence of the n_e, T_e and T_i profiles.

Figure 3(a)-(c) indicates the change in the core and

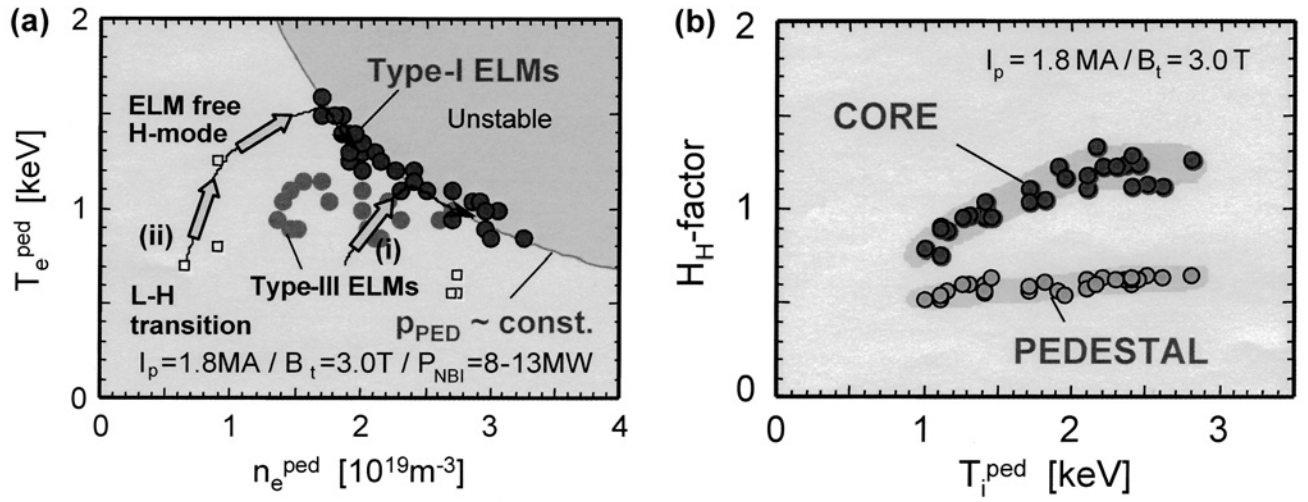

Fig. 2 (a) Diagram of electron density and temperature at the H-mode pedestal shoulder for classifying ELM behavior in JT-60U. (b) Influence of the pedestal temperature on the core and pedestal energy confinement in the type-I ELMy H-mode plasmas on JT-60U. The H_H-factors are evaluated by the ONL scaling.

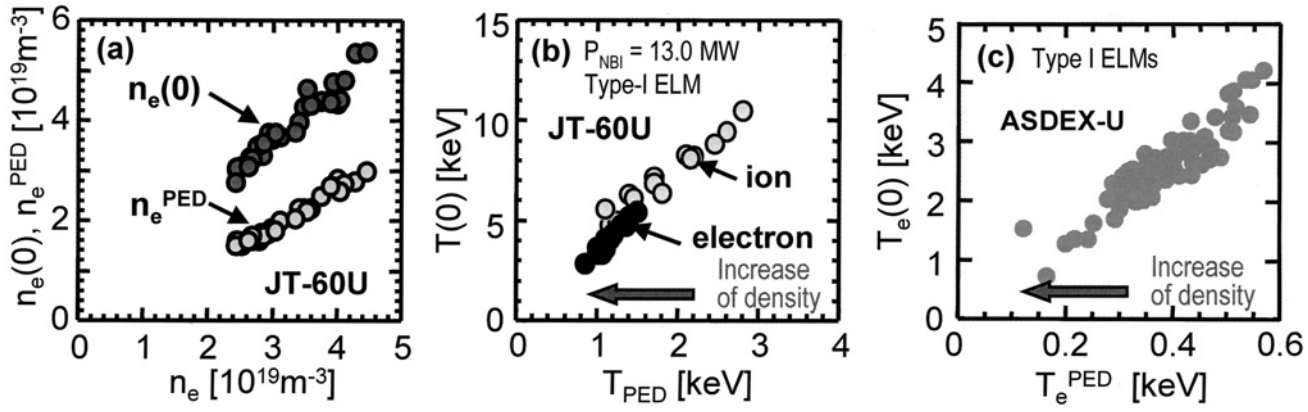

Fig. 3 (a) Central and pedestal electron densities as a function of the line-averaged electron density in JT-60U. (b) Electron and ion temperature at the plasma center as a function of the pedestal temperature in JT-60U. (c) Central electron temperature as a function of the pedestal temperature in ASDEX Upgrade.

pedestal density and temperature with varying plasma density. The density and temperature profiles in the plasma core show the tendency expected from the results described in Sec. **2.2**. When the plasma density is raised by gas puff, both the central and pedestal densities are increased together as shown in Fig. 3(a). On the other hand, it can also be seen for each species that the temperature profiles are approximately self-similar and differ only by a constant factor throughout a wide range of densities in the type-I ELMy H-mode plasmas on both JT-60U and ASDEX Upgrade, as shown in Figs. 3(b) and (c), respectively. It can be easily shown that this result is consistent with the saturation of W_{th} for the increase of plasma density. In practice, the thermal pressures at the plasma center $p(0)$ are almost constant independent of the variation of density (e.g, $p(0) \sim 6\times10^4$ Pa for the case of JT-60U shown in Figs. 3(a) and (b)).

We can summarize the results obtained for the density dependence of the energy confinement as follows. The edge pedestal temperature plays a significant role as a boundary condition in determining the core energy confinement (see Fig. 2(b)). When the density is increased, the saturation of p_{ped} during the type-I ELMy H-mode regime forces a reduction in the temperature, as shown in Fig. 2(a). The core temperature in turn decreases by an approximately constant factor with a reduction in the temperature at the boundary (see Figs. 3(b) and (c)).

It follows from these results that the energy confinement degradation at high densities could be overcome by raising the pedestal temperature. In practice, there seem to be two main methods for sustaining a high pedestal temperature. The first is to operate in ELMy H-mode at high triangularity configuration. The above results naturally suggest that, if a higher sustainable p_{ped} is produced in type-I ELMy H-mode discharges, the pedestal temperature is expected to become higher at a given density (see Fig. 4(a)), and a higher energy confinement enhancement factor would be obtained [20]. High triangularity discharges have been shown to lead to a higher edge pedestal pressure due to the improvement of the edge MHD stability limit, as shown in Fig. 4(b). The other method is to rely on the density profile control. By controlling the peak density profile, we can realize a relative decrease in the peripheral density at fixed averaged density. Externally puffed seed impurity leads to the center-peaked density profiles as well as a slight reduction in the thermal ion density due to the dilution of deuterium [21]. Figure 4(c) shows the electron density profiles in ELMy H-mode plasmas with and without argon gas injection in JT-60U. Density profile peaking is seen in the argon-injected case, and thus the edge density relatively becomes lower than that in the case using deuterium gas alone.

Figures 5(a) and (b) show the ion temperature profiles for the cases of high triangularity and argon-injected ELMy H-mode plasmas. It can be clearly seen that the edge pedestal temperature is raised by each operation method, compared to the discharges at low triangularity and with only deuterium gas. Similarly to the characteristics of the temperature profile shown in Figs. 3(b) and (c), the core profiles of temperature are seen to be self-similar as plotted in the logarithmic scale in Fig. 5. These results imply that there is a minimum scale length of temperature gradient and the energy transport adjusts itself to maintain this scale length [19,22]. In Figs. 5(a) and (b), the core temperatures are varied according to a vertical offset of the profiles on a log scale, in which changing the boundary temperatures at constant gradient scale length results in self-similar core profiles.

3. The Role of the Pedestal Structure in ELM Energy Loss

Among the several types of ELMs, high energy confinement with sufficiently high fusion power gain is in many cases accompanied by type-I ELMs. The type-I ELM, which appears when a sufficiently high level of additional

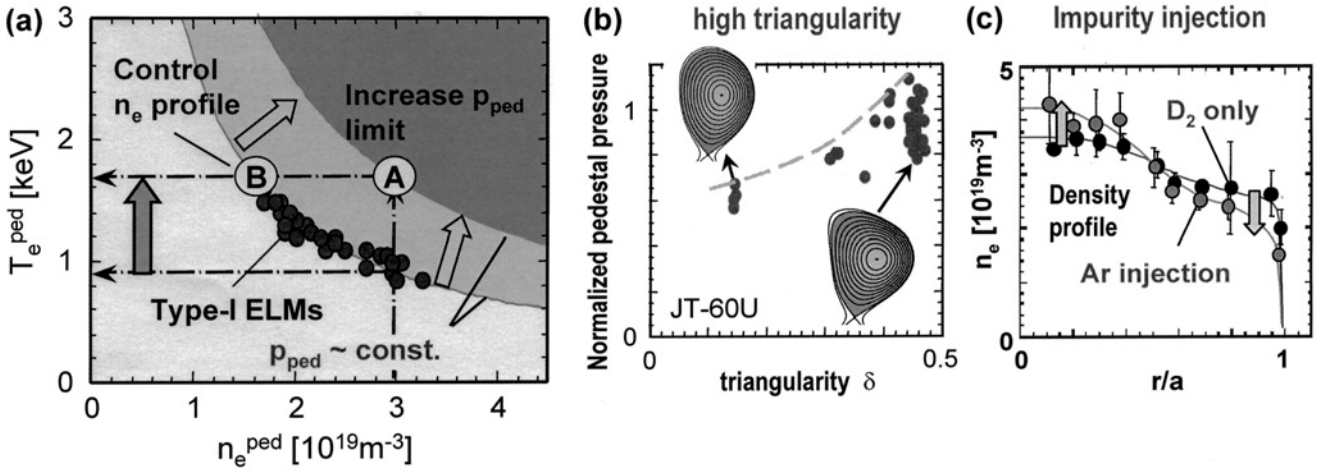

Fig. 4 (a) Schematic representation of the operation methods to sustain a higher pedestal temperature; (A) high triangularity configuration, (B) density peaking by impurity injection. (b) Normalized pedestal pressure (p_{ped}/p_{ped}^{ONL}) as a function of triangualrity in JT-60U (c) Electron density profiles for the cases with and without argon injection at fixed line-averaged density.

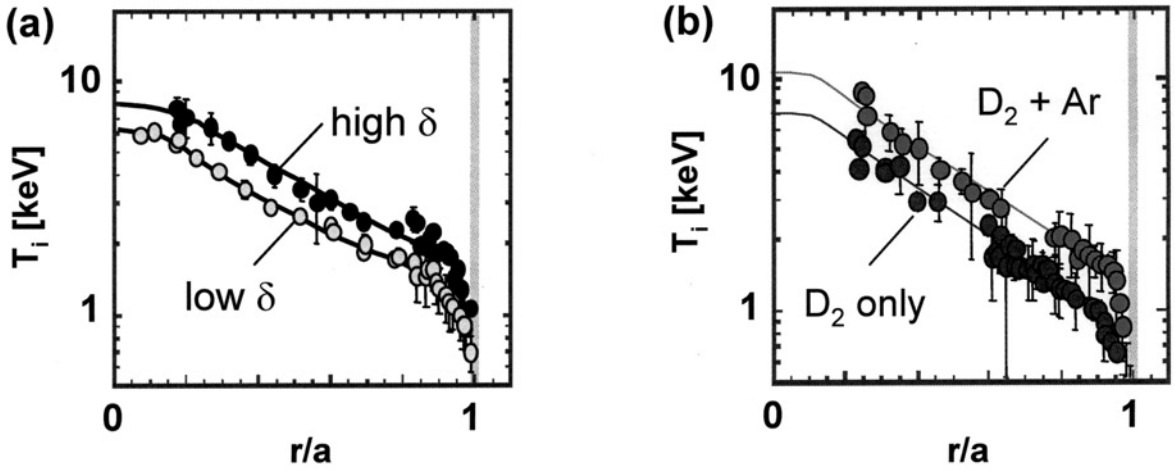

Fig. 5 Profile similarity during the type-I ELMy H-mode plasmas: (a) high triangularity discharges, (b) argon injected discharges. Both cases show the increase of the pedestal temperature and analogous core temperature profiles.

power is applied, is characterized by a repetition frequency that increases in proportion to the power [1], and ELMs of this type generate the largest energy loss from the main plasma. Thus, type-I ELMs with high pedestal temperature may violate the energy impact limit of plasma facing components. Mitigating the heat load onto the divertor target without deteriorating the energy confinement has been a critical goal in recent ELM studies performed to achieve highly integrated performance of fusion reactor. For the divertor design of ITER, the melting and ablation threshold requires that the peak heat load does not exceed the technological feasible maximum of ~ 0.5 MJ/m^2 at the divertor plate with the deposition time of 0.1 ms, or ~ 1.2 MJ/m^2 with 1.0 ms [11]. These requirements set the maximum ELM energy loss ΔW_{ELM} to ~ 6 MJ in ITER design. From the viewpoint of the energy confinement, the higher pedestal stored energy W_{ped} is required, as presented in Sec. **2**. However, as a basic observation, ELM energy loss can become larger in H-mode plasmas with high pedestal stored energy [23]. Figure 6 shows the relation of ΔW_{ELM} and W_{ped} investigated in JT-60U and ASDEX Upgrade. It can be seen that ΔW_{ELM} assumes values up to a certain fraction of W_{ped}, i.e., $\Delta W_{ELM}/W_{ped} \leq 0.1$. Since the ELM is essentially a relaxation of the steep pressure gradient that occurs at the pedestal, it can be expected that ΔW_{ELM} is bounded by a fraction of W_{ped}. It should be noted from Fig. 6 that there is a variation of ELM size at a given W_{ped}. In this Section, we examine the variations of ΔW_{ELM} with the pedestal parameters, assuming ΔW_{ELM} can be expressed as $\Delta W_{ELM} = W_{ped} \cdot f(\nu^*, \rho^*, \beta, \varepsilon, \delta, \ldots)$.

Experimentally, it is seen in many cases that the ELM frequency f_{ELM} increases and the ELM energy loss ΔW_{ELM} decreases when the plasma density is raised. Figures 7(a) and (b) show the ELM energy loss normalized to the pedestal stored energy $\Delta W_{ELM}/W_{ped}$ as a function of the normalized pedestal collisionality ν_{ped}^* for the discharges in JT-60U and ASDEX Upgrade, respectively. The normalized pedestal

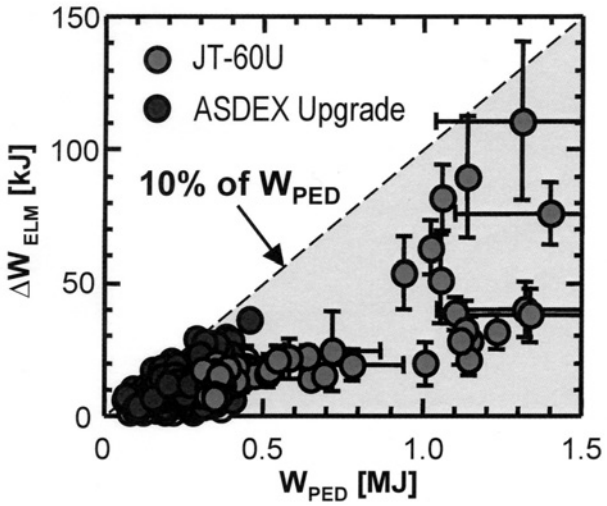

Fig. 6 Relation between ELM energy loss and pedestal stored energy in JT-60U and ASDEX Upgrade. The broken line corresponds to 10% of the pedestal stored energy.

collisionality ν_{ped}^* is defined as $\nu_{ped}^* \equiv \pi R_p q_{95}/\lambda_{ee}$, where λ_{ee} denotes the electron-electron collision mean free path. Discharges were performed in both cases at I_p = 1 MA, with the power crossing the separatrix P_{sep} ~ 4 MW. In the case of JT-60U, the normalized pedestal Larmor radius ρ_{pol}^{ped*} ~ 0.04 and the pedestal poloidal beta β_{pol}^{ped} ~ 0.2 in the fixed plasma configuration. In the case of ASDEX Upgrade, we have ρ_{pol}^{ped*} ~ 0.02 and β_{pol}^{ped} ~ 0.5 for both the low and high triangularity cases (δ_u ~ 0.0 and δ_u ~ 0.2). It can be seen for both devices that in the fixed configuration the ELM size ($\Delta W_{ELM}/W_{ped}$) decreases with ν_{ped}^*. The ELM behavior at higher ν_{ped}^* in JT-60U also shows higher ELM frequency f_{ELM} and smaller ELM energy loss ΔW_{ELM} than those in the case of lower ν_{ped}^* (see Fig. 7(a)). In ASDEX Upgrade, we also find an explicit difference of $\Delta W_{ELM}/W_{ped}$ between lower and higher triangularity at fixed ν_{ped}^*, as shown in Fig. 7(b). The higher triangularity plasmas obviously produce two- to

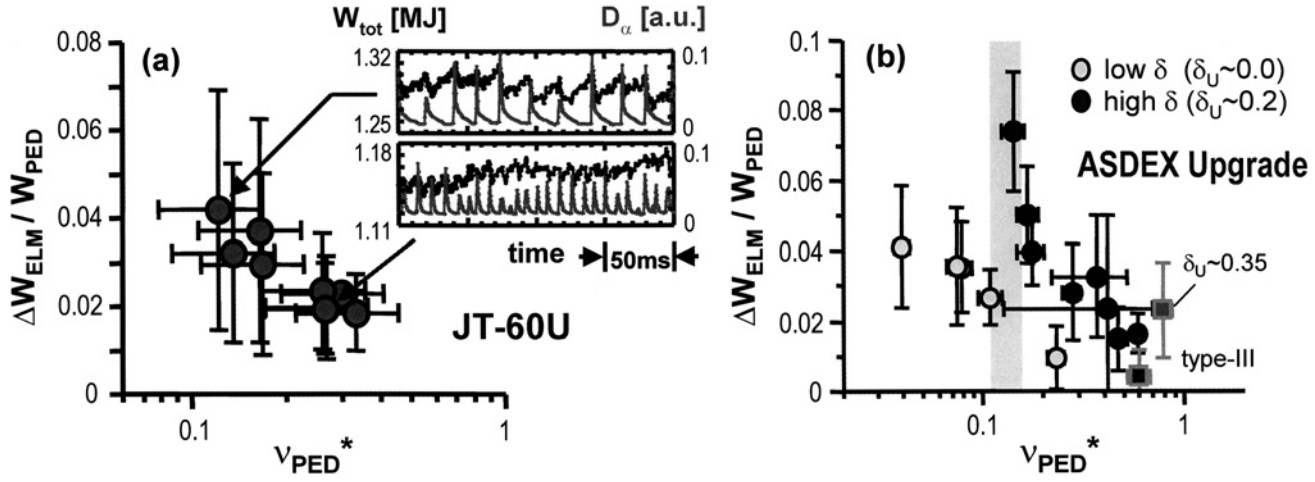

Fig. 7 Dependence of normalized ELM energy loss ($\Delta W_{ELM}/W_{PED}$) on normalized pedestal collisionality (ν_{PED}*) in (a) JT-60U (δ = 0.3) and (b) ASDEX Upgrade (δ = 0.0, 0.2). Shown in both figures are discharges performed at I_P = 1 MA and P_{SEP} = 4 MW.

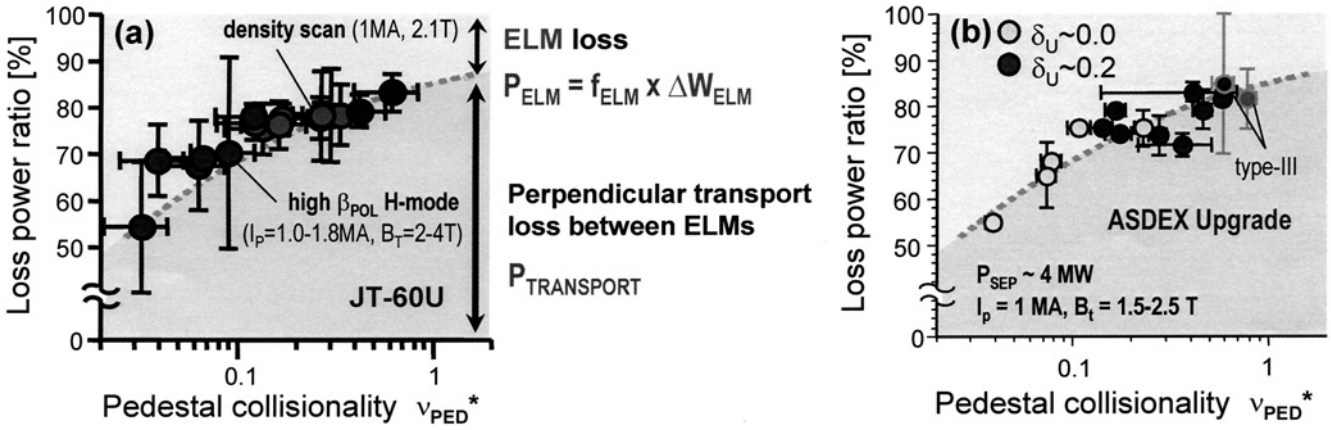

Fig. 8 The fraction of the power assigned to ELM and perpendicular transport between ELMs based on the power crossing the separatrix in (a) JT-60U and (b) ASDEX Upgrade.

fourfold larger ELM losses than the lower triangularity case. When evaluating the relative changes of the T_e profiles due to an ELM measured with the ECE radiometer, we find that the larger ELM energy drop at higher triangularity involves an ELM perturbation that extends radially more inward than that in the lower triangularity case [23].

In a time scale that is much longer than an ELM event that periodically generates a similar level of energy loss, the ELMy H-mode can be operated in a steady state, i.e., $\overline{dW/dt} = 0$, where the bar denotes the averaged value over ELM cycles. Therefore, the relation between the energy confinement and ELM losses can be discussed from the viewpoint of the energy balance equation.

Near the plasma boundary, the following energy balance holds:

$$\frac{dW}{dt} = P_{sep} - P_{transport} - \left(\frac{dW}{dt}\right)_{ELM} \cdot \delta(t - t_{ELM}), \quad (2)$$

where $P_{transport}$ denotes the perpendicular transport loss between ELMs, $(dW/dt)_{ELM}$ and t_{ELM} are the time derivative of plasma energy at an ELM burst and the time when the ELM crash occurs, respectively. In a steady state situation, $\overline{dW/dt} = 0$ and thus P_{sep} is assigned to two loss channels of the inter-ELM loss power $P_{transport}$ and ELM loss power P_{ELM} ($= f_{ELM} \times \Delta W_{ELM}$) [23]. Figures 8(a) and (b) show the fraction of the power assigned to P_{ELM} and $P_{transport}$ from P_{sep} in JT-60U and ASDEX Upgrade, respectively (i.e., the loss power ratio of 100 % corresponds to P_{sep}). It has previously been observed that P_{ELM} is 20–40 % of P_{sep} in type-I ELMy H-modes. However, this result indicates that this loss power ratio can be changed by the pedestal collisionality. These figures amount to saying that, when ν_{ped}* is increased, the inter-ELM transport at the plasma edge is enhanced and the ELM transported loss is reduced, independently of the plasma configuration. From Figs. 7 and 8, one can find that it is not simple to achieve the high energy confinement simultaneously with small ELM losses. As shown in Fig. 7, ΔW_{ELM} becomes smaller with increasing ν_{ped}*. However, small transport loss (or good confinement) is always accompanied by a large ELM loss power at low ν_{ped}* (see Fig. 8). On the other hand, when

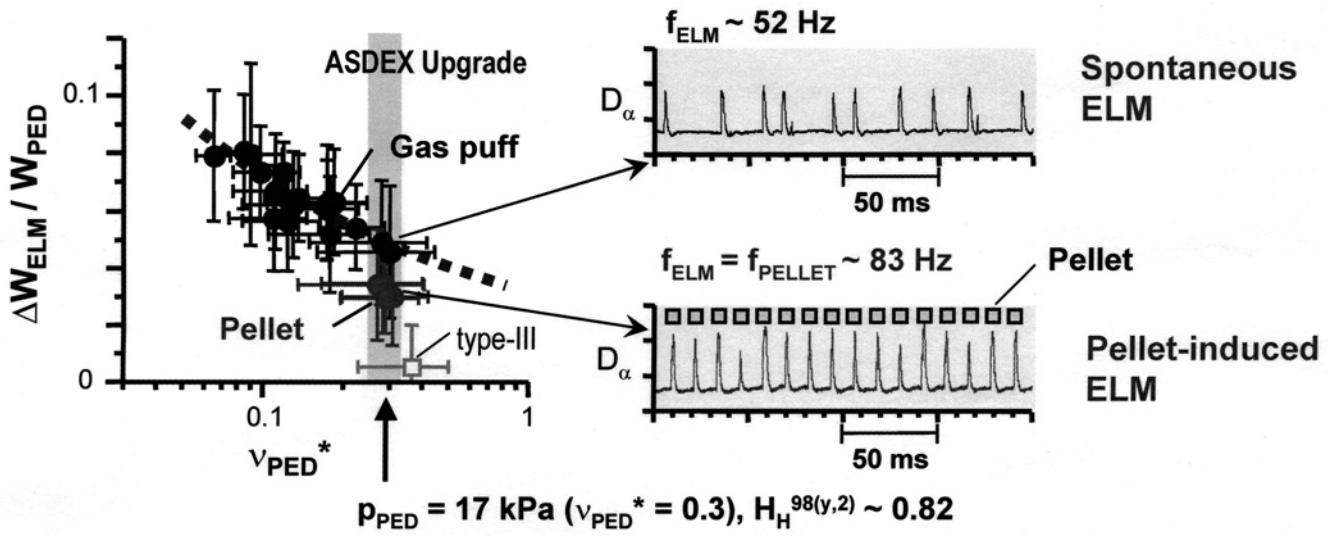

Fig. 9 Dependence of $\Delta W_{ELM}/W_{PED}$ on ν_{PED}* for the discharges with and without pellet injection performed at I_P = 1 MA, B_T = 2.7–3.0 T and P_{NB} = 5–7 MW. The D_α emission signals in the phases at the identical pedestal conditions are also shown.

a small ELM loss power is assigned, the energy confinement is not favorable at high ν_{ped}*. In the existing ITER design, since it has been envisaged that the operation will be performed at lower ν_{ped}* (~ 0.05), a non-dimensional analysis involving the other parameters, such as ρ_{pol}^{ped}* and β_{pol}^{ped}, will be needed.

However, several operation methods have been examined for mitigation of ELM losses at a given energy confinement quality in ASDEX Upgrade and JT-60U. In ASDEX Upgrade, a fully controlled scenario with favorable divertor conditions has been achieved by maintaining a constant ELM frequency enforced by injection of small pellets [24]. Pellet injection is known to trigger ELMs and thus is being considered as a desirable technique for external control of the ELM frequency [25-29]. It is certainly clear that injected pellets reduce ΔW_{ELM} when the pellet repetition frequency f_{pellet} exceeds the spontaneous ELM frequency. However, since each pellet has a finite mass, the pedestal density or ν_{ped}* is raised by the effect of pellet fuelling. For this reason, it has been uncertain whether the reduction of ΔW_{ELM} is possible at a given ν_{ped}*. We therefore conducted experiments to achieve equivalence of the pedestal conditions between pellet injection and gas puff methods. Figure 9 shows $\Delta W_{ELM}/W_{ped}$ as a function of ν_{ped}* for the discharges with and without pellet injection performed at I_p = 1 MA, B_t = 2.7–3.0 T, δ_u ~ 0.1 and P_{NB} = 5–7 MW in ASDEX Upgrade. While $\Delta W_{ELM}/W_{ped}$ decreases continuously with an increase in ν_{ped}* in the case of the natural type-I ELMy H-mode, it is found that the pellet-triggered ELM energy losses are smaller by ~ 35 % than those of natural ELMs at ν_{ped}* ~ 0.3 [30]. Since the pedestal conditions are identical (p_{ped} ~ 17 kPa, ν_{ped}* ~ 0.3), the energy confinement qualities are also the same at the H_H-factor of 0.82, as described in Sec. **2**. Therefore, this result proves that the active control of ELM frequency with pellets can be a useful technique for the mitigation of ELM energy loss while maintaining a constant energy confinement. However, large pellets play a role of refuelling as well as triggering ELM, leading to the confinement degradation by increased density. The access to a lower density regime is the next issue in the pellet-controlled scenario. It may be worth pointing out in passing that the difference of the absolute values of $\Delta W_{ELM}/W_{ped}$ for type-I ELMs between Figs. 7(b) and 9 implies that $\Delta W_{ELM}/W_{ped}$ cannot simply be expressed by ν_{ped}* (e.g, q_{95} = 3.5–4.0 in Fig. 7(b) and q_{95} ~ 5.0 in Fig. 9) as described in the first half of this Section.

As shown in Fig. 8, higher energy confinement can be achieved at lower ν_{ped}*. However, ELMy H-modes in the lower ν_{ped}* regime are basically accompanied by large ELM with low frequency. For a highly integrated performance, a small ELM with high frequency is strongly desired at lower ν_{ped}*. In JT-60U, the grassy ELM regime is drawing the attention as a promising operation to realize highly integrated performance of high energy confinement with small ELMs in the low ν_{ped}* regime [31]. The pure grassy ELMs can appear at high q_{95} ($\geq$ 5) and high δ ($\geq$ 0.5), and their appearance is made more likely by a high β_{pol} value ($\geq$ 1.6). In the grassy ELMy H-mode regime, the ELM frequency becomes significantly high, on the order of kHz, and $\Delta W_{ELM}/W_{ped}$ becomes less than 1% at ν_{ped}* ~ 0.03, where P_{ELM}/P_{sep} remains 30–50 %. On the other hand, in the type-I ELMy H-mode regime, $\Delta W_{ELM}/W_{ped}$ is estimated to become ~10 % or larger (P_{ELM}/P_{sep} ~ 45 %) at ν_{ped}* ~ 0.03 when high energy confinement is sustained at higher triangularity. Since the existing ITER design is characterized by an operating pedestal collisionality around ν_{ped}* ~ 0.03, the energy loss of grassy ELMs is at an acceptable level in ITER. For easier generation of grassy ELMs, the extension of the operation regime at lower q_{95} and δ is currently being investigated in JT-60U.

4. Conclusions

The roles of the pedestal structure in ELMy H-mode plasmas for the core energy confinement and for the ELM

energy losses have been investigated in JT-60U and ASDEX Upgrade. The confinement degradation seen at higher densities is attributed to the reduction of the pedestal temperature limited by the ELM activities and the stiffness of the temperature profiles. In high triangularity or impurity seeded H-modes, in which higher energy confinement is generally achieved, a higher pedestal temperature is obtained by improving the edge MHD stability or the density profile peaking, respectively. The upper bound of the ELM energy loss is characterized by the pedestal energy. The ELM energy loss can become smaller at fixed pedestal energy when the pedestal collisionality is raised. When the pedestal collisionality is increased, the energy transport between ELMs is enhanced and the ELM loss power fraction is reduced. It is also shown in ASDEX Upgrade that continuous pellet injection is an effective means of mitigating ELM losses while maintaining the core confinement quality. In JT-60U, the operation regime of grassy ELM is being investigated as a promising operation for the goal of achieving highly integrated performance of high energy confinement with small ELMs in the low collisionality regime.

References

[1] H. Zohm, Plasma Phys. Control. Fusion **38**, 105 (1996).
[2] H. Zohm, Plasma Phys. Control. Fusion **38**, 1213 (1996).
[3] J.W. Connor, Plasma Phys. Control. Fusion **40**, 191 (1998).
[4] J.W. Connor, Plasma Phys. Control. Fusion **40**, 531 (1998).
[5] M.R. Wade *et al.*, Nucl. Fusion **38**, 1839 (1998).
[6] H.S. Bosch *et al.*, J. Nucl. Mater. **266-269**, 462 (1999).
[7] A. Sakasai *et al.*, J. Nucl. Mater. **266-269**, 312 (1999).
[8] M. Groth *et al.*, Nucl. Fusion **42**, 591 (2002).
[9] R. Aymar *et al.*, Nucl. Fusion **42**, 519 (2002).
[10] ITER Physics Basis Expert Groups on Divertor and Divertor Modelling and Database, ITER Physics Basis Editors, Nucl. Fusion **39**, 2391 (1999).
[11] A. Leonard *et al.*, J. Nucl. Mater. **266-269**, 109 (1999).
[12] G. Janeschitz *et al.*, J. Nucl. Mater. **290-293**, 1 (2001).
[13] A. Loarte *et al.*, in Fusion Energy 2000 (*Proc. 18th Int. Conf.* Sorrent, 2000) IAEA, Vienna, ITERP/11(R) (2000).
[14] JET Team, Nucl. Fusion **39**, 1687 (1999).
[15] W. Suttrop *et al.*, in Fusion Energy 1998 (*Proc. 17th Int. Conf.* Yokohama, 1998) Vol. 2, IAEA, Vienna, 777 (1999).
[16] N. Asakura, Plasma Phys. Control. Fusion **39**, 1295 (1997).
[17] T. Takizuka, Plasma Phys. Control. Fusion **40**, 851 (1998).
[18] H. Urano *et al.*, Nucl. Fusion **42**, 76 (2002).
[19] W. Suttrop *et al.*, Plasma Phys. Control. Fusion **39**, 2051 (1997).
[20] H. Urano *et al.*, Plasma Phys. Control. Fusion **44**, 11 (2002).
[21] H. Urano *et al.*, J. Plasma Fusion Res. SERIES, Vol. 4, 239 (2001).
[22] H. Urano *et al.*, Plasma Phys. Control. Fusion **44**, A437 (2002).
[23] H. Urano *et al.*, Plasma Phys. Control. Fusion **45**, 1571 (2003).
[24] P.T. Lang *et al.*, Nucl. Fusion **44**, 665 (2004).
[25] P.T. Lang *et al.*, Nucl. Fusion **36**, 1531 (1996).
[26] G.L. Jackson *et al.*, Phys. Rev. Lett. **67**, 3098 (1991).
[27] L.R. Baylor *et al.*, Phys. Plasmas **7**, 878 (2000).
[28] L.R. Baylor *et al.*, J. Nucl. Mater. **290-293**, 398 (2001).
[29] H. Takenaga *et al.*, Phys. Plasmas **9**, 2217 (2001).
[30] H. Urano *et al.*, Plasma Phys. Control. Fusion **46**, A315 (2004).
[31] Y. Kamada *et al.*, Plasma Phys. Control. Fusion **44**, A279 (2002).